Structural and Vibrational Properties of Trehalose: A Density Functional Study

P. Ballone,*,†,‡ M. Marchi,§ C. Branca,† and S. Magazú†

Istituto Nazionale per la Fisica della Materia and Dipartimento di Fisica, Universitá degli Studi di Messina, Contrada Papardo, C.P. 50, 98166 Messina, Italy, Section de Biophysique des Protéines et des Membranes, DBCM, DSV, CEA, Centre d'Études, Saclay, 91191 Gif-sur-Yvette Cedex, France, and Institut für Festkörper Forschung, Forschungszentrum Jülich, D-52425 Jülich, Germany

Received: December 9, 1999; In Final Form: April 13, 2000

We apply density functional theory in the gradient-corrected local-density approximation to the determination of structural properties and harmonic vibrational modes of trehalose in the gas phase and in the monohydrate crystal. We analyze the local conformation and the relative strength of intra- and intermolecular hydrogen bonds, and we discuss the effects of the crystal environment on the molecular geometry and vibrational frequencies. The density functional results are used to assess the quality of a recent molecular mechanics model. This simplified scheme provides a fairly good description of ground-state geometries, while vibrational properties are only in qualitative agreement with those computed by the density functional method.

Introduction

Trehalose, a glucose disaccharide, is an important metabolic compound present in sizable amount in fungi, plants, and insects.[1] It is known to provide effective antifreezing and antidehydration protection to biological cells, and for this reason, it is extensively used in food processing, and increasingly exploited in pharmacology and biomedical applications. These reasons of interest have motivated the intensive investigation of structural, dynamical, and chemical properties of this molecule in a variety of different phases and environments. While the detailed mechanism for the preservation of biological structures by trehalose is still the subject of debate, the trehalose−water system (in the crystal, glassy, and liquid solution phases) is now well characterized by experiments, and can serve as a crucial benchmark for the modeling of this molecule, in view of atomistic studies of its physical chemistry properties,[2] and biological activity.[3]

In our study, we apply density functional theory (DFT) to the determination of structural and vibrational properties of a crystal form of trehalose monohydrate and of the gas-phase trehalose molecule. The aim of our computation is 2-fold: first, we analyze, by a reliable and parameter free method, the structural features and the relative strength of intra- and intermolecular hydrogen bonds, and we determine their specific signature on the vibrational spectra; second, we provide an extensive set of structural and dynamical data to test and refine molecular mechanics models of trehalose and trehalose−water systems.

We base our structural study on the recent experimental data on the $\alpha-\beta$ trehalose monohydrate crystal:[10] we start the atomic relaxation for the crystal from the experimental positions, and also the initial configuration for the gas-phase molecule is extracted from the experimental crystal structure. We underline that we did not attempt a global optimization of the structure, or a systematic search for the different isomers. Nevertheless, the size of the molecule, the variety of intra- and intermolecular bonds present in the monohydrate crystal, and the possibility of performing computer experiments (as detailed below) already offer an extended set of data and local conformations to characterize the potential energy surface of this system.

We complete our study by comparing our DFT data with the results of a recent empirical potential model,[17] and we refine a set of interatomic potential parameters tuned on the DFT data.

Computational Method

The electron ground-state energy E_t as a function of the atomic coordinates $\{\mathbf{R_I}\}$ is computed within density functional theory[4] with the gradient-corrected approximation of Perdew, Burke, and Ernzerhof[5] for the exchange and correlation energy. This approximation has been chosen because it is known to provide a fairly accurate description of hydrogen bonds.[6] In our computation only valence electrons are treated explicitly, and their interaction with the ionic cores is described by soft pseudopotentials of the Troullier−Martins type.[7] The Kohn−Sham orbitals are expanded on a basis of plane waves, with a kinetic energy cutoff of 70 Ry. In the case of the crystal, the first Brillouin zone is sampled at the Γ-point only. In view of the insulating character of this compound, and of the relatively large size of the unit cell (96 atoms), this approximation is expected to have negligible influence on the computed properties. In the case of the gas-phase molecule, the volume of the periodically repeated unit cell ($V = 9500$ Å^3) is such that the interaction of the central molecule with the periodic replicas is negligible.[8]

The atomic positions are relaxed by the DFT−molecular dynamics scheme of Car and Parrinello.[9] The relaxation is continued until the residual forces on the atoms drop below a preassigned threshold, which in the present computation is set to 10^{-5} in atomic units.

Vibrational eigenvalues and eigenvectors are obtained by diagonalization of the dynamical matrix. The second derivatives of the potential energy surface with respect to the atomic positions have been computed by a simple finite differences approximation.

† Istituto Nazionale per la Fisica della Materia and Universitá degli Studi di Messina.
‡ Institüt für Festkörper Forschung.
§ DBCM, DSV, CEA, Centre d'Etudes.

10.1021/jp994346b CCC: $19.00
Published on Web 06/13/2000

CHART 1: Structure of the Trehalose Molecule

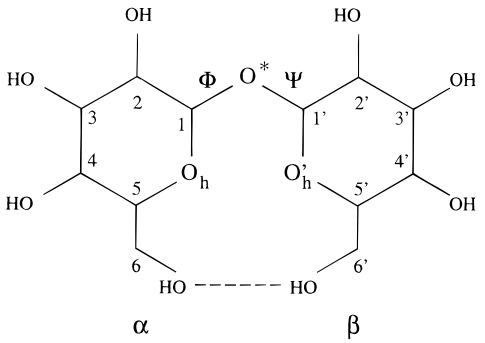

TABLE 1: Selected Interatomic Distances (Å) and Angles (deg) in a Gas-Phase α−*β* Trehalose Molecule (First Line) and in the Monohydrate Crystal (Second Line, in Parentheses)[a]

atoms	distance	atoms	distance
O*−C1	1.432	O*−C1′	1.414
	(1.428)		(1.412)
C1−C2	1.537	C1′−C2′	1.532
	(1.531)		(1.539)
C2−C3	1.531	C2′−C3′	1.523
	(1.531)		(1.534)
C3−C4	1.529	C3′−C4′	1.527
	(1.529)		(1.539)
C4−C5	1.544	C4′−C5′	1.535
	(1.540)		(1.533)
C5−C6	1.515	C5′−C6′	1.522
	(1.518)		(1.521)
C1−O_h	1.416	C1′−O_h′	1.425
	(1.434)		(1.434)
C2−O	1.446	C2′−O′	1.438
	(1.425)		(1.430)
C3−O	1.432	C3′−O′	1.441
	(1.444)		(1.438)
C4−O	1.436	C4′−O′	1.436
	(1.440)		(1.438)
C5−O_h	1.457	C5′−O_h′	1.453
	(1.460)		(1.444)
C6−O	1.443	C6′−O	1.425
	(1.444)		(1.434)

atoms	angle	atoms	angle
C1−O*−C1′	115.5		
	(113.7)		
C1−O_h−C5	114.0	C1′−O_h′−C5′	111.7
	(114.5)		(112.0)
C2−C1−O_h	109.8	C2′−C1′−O_h′	109.4
	(109.6)		(110.0)
C4−C5−O_h	111.6	C4′−C5′−O_h′	109.5
	(111.0)		(109.6)
C2−C1−O*−C1′ (Φ)	191.0	C2′−C1′−O*−C1 (Ψ)	149.1
	(190.3)		(148.8)
O−C6−C5−O_h	76.7	O′−C6′−C5′−O_h′	71.0
	(79.8)		(74.4)

[a] Atom numbers are defined in Chart 1.

Gas-Phase Molecule

As a first step, we relax the structure of an isolated molecule (see Chart 1; the oxygen and hydrogen atoms adopt the same label as the nearest carbon atom), starting from the atomic coordinates of a trehalose molecule in the monohydrate crystal, given in ref 10. Representative interatomic distances and angles in the relaxed structure are reported in Table 1.

Since the two rings belong to two different (α and *β*) anomeric forms, it is not surprising to find that distances and angles measured on one ring differ slightly from the corresponding structural parameters on the other ring.

TABLE 2: Atomic Charges Reproducing the Molecular Electrostatic Potential[a]

atoms	charge (e)	atoms	charge (e)	atoms	charge (e)
$H1_C$=$H1'_C$	0.034	$H3_{OH}$=$H3'_{OH}$	0.365	O6=O6′	−0.578
$H2_C$=$H2'_C$	0.050	$H4_{OH}$=$H4'_{OH}$	0.341	C1=C1′	0.341
$H3_C$=$H3'_C$	0.009	$H5_{OH}$=$H5'_{OH}$	0.355	C2=C2′	0.030
$H4_C$=$H4'_C$	0.048	O*	−0.349	C3=C3′	0.390
$H5_C$=$H5'_C$	0.059	O2=O2′	−0.555	C4=C4′	0.130
$H6_{CH_2}$=$H6'_{CH_2}$	0.022	O3=O3′	−0.616	C5=C5′	0.102
$H7_{CH_2}$=$H7'_{CH_2}$	0.022	O4=O4′	−0.557	C6=C6′	0.235
$H2_{OH}$=$H2'_{OH}$	0.350	O_h=O'_h	−0.384		

[a] Carbon atoms are numbered according to Chart 1; hydogen and oxygen atoms take the number of the nearest C atom; the C, OH, and CH_2, subscripts identify hydrogen atoms bonded to C and O atoms or belonging to the CH_2 group, respectively.

Despite the careful relaxation, and the large number of hydroxyl groups attached to adjacent carbon atoms in the glucopyranose rings, we observe only one apparent intramolecular hydrogen bond (O6′−H6′−O6), joining the two CH_2OH terminations of glucose. The structural results show that even this bond is far from ideal (d(O6′−H6′) = 0.99 Å, d(H6′−O6) = 1.94 Å, O6′−H6′−O6 = 156.0°, giving an O6−O6′ distance of 2.87 Å). To estimate the strength of this bond, we rotate the O6′−H6′ group by 90° around the C6′−C5′ axis.[20] In this way we observe an energy increase of 5 kcal/mol, which we identify with the energy associated with this bond.

All the other hydroxyl groups display a tendency to a tangential orientation with respect to the rings (clockwise in the α ring, counterclockwise in the *β* ring), which suggests the presence of a weak interaction with the nearest oxygen atom. Distances (d(O−H) ≥ 2.34 Å) and angles ($\theta \leq 110°$), however, are far from those of a true hydrogen bond.

Both rings are characterized by a strong anomeric effect, revealed by a sizable asymmetry in the C1−O_h and C5−O_h distances (and C1′−O_h′ and C5′−O_h′ distances), and in the deviation of the bond angles from the ideal values around the hemiacetal oxygens (see Table 1).

The electrostatic potential around the molecule is computed in reciprocal space from the total (i.e., ions plus electrons) valence charge via Poisson's equation, and transformed in real space on the same grid used for the computation of the Kohn−Sham orbitals and electron density. A set of effective atomic charges is determined by a least-squares fit to the electrostatic potential for the grid points in which the valence charge is negligible, following a standard procedure[11] implemented in the DFT code that we used.[8] Those charges, often used to represent the electrostatic interactions in molecular mechanics models, appear to be rather similar for corresponding atoms in the two glucose rings, and we report in Table 2 their arithmetic average. We observe that the oxygen atom with the lowest charge (in absolute value) is the bridging oxygen O*, followed by the two hemiacetal oxygens, which are also connected to two carbon atoms.

As mentioned in the previous section, vibrational eigenvalues and eigenvectors have been computed by diagonalization of the dynamical matrix. The infrared activity of each mode at frequency ν_j has been evaluated by the approximate expression[12]

$$\alpha(\nu_j) = \frac{8\pi^3 \nu_j}{3ch} \left| \sum_I q_i \delta \mathbf{r}_I^{(j)} \right|^2$$

where $\delta \mathbf{r}_I^{(j)}$ is the displacement of atom I for the jth vibrational eigenvector, and q_i are the effective atomic charges discussed

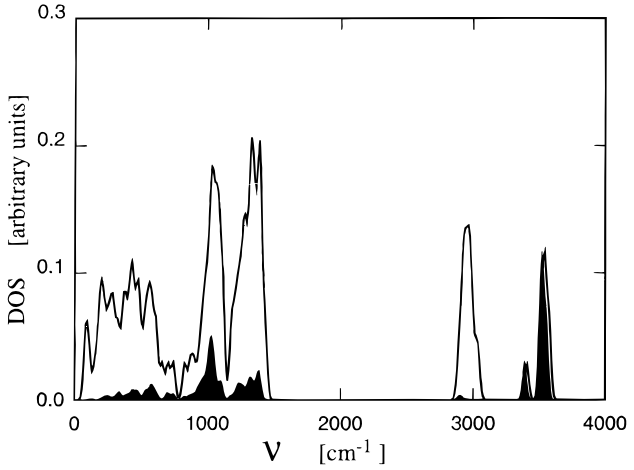

Figure 1. Vibrational spectrum of the gas-phase trehalose molecule. The infrared activity is given by the black area under the lower curve.

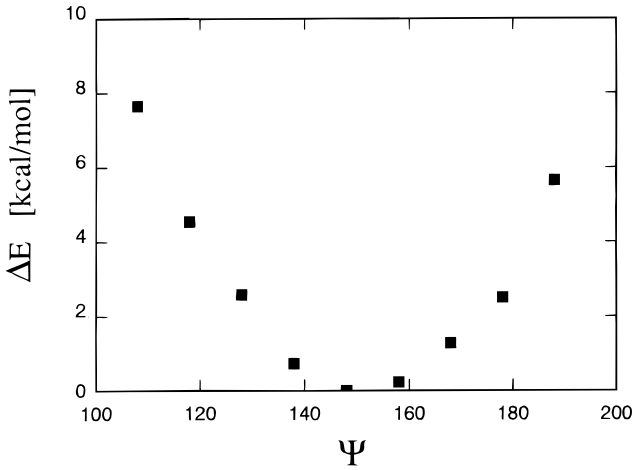

Figure 2. Potential energy of the gas-phase trehalose molecule as a function of the Ψ torsional angle (see Chart 1). All other degrees of freedom are optimized. The zero of the energy corresponds to the ground-state structure.

above. In order of decreasing frequency, first we find a narrow band (from 3502 to 3558 cm^{-1}) of O−H stretching for the groups not involved in the intramolecular hydrogen bond. At significantly lower frequency (3388 cm^{-1}) we find the stretching mode of the O6′−H6′ group, joined to O6 by the hydrogen bond described above. The stretching modes of the C−H bonds are found at a frequency between 2874 and 3023 cm^{-1}, separated by a large gap from the band of the hybridized H−C−H, C−C−H, and C−O−H bending modes, observed between 1175 and 1433 cm^{-1}. The stretching of the C−O bonds occurs in a range between 970 and 1100 cm^{-1}, while it is difficult to assign a well-defined character to most of the modes below ∼950 cm^{-1}: only the oscillations of the OH groups around the minimum of the C−C−O−H torsional potential are well localized and fairly easy to identify. These modes have an energy between 420 and 570 cm^{-1}, with the exception of the OH group giving rise to the intramolecular hydrogen bond, whose torsional mode has an energy of 700 cm^{-1}. The total and infrared-active vibrational densities of states are reported in Figure 1.

The conformational freedom in trehalose is mainly due to changes in the torsional angles centered on the C1−O* and O*−C1′ bonds (indicated by Φ and Ψ in Chart 1). To evaluate the force constant associated with these degrees of freedom, we computed the energy of the trehalose molecule upon changing the angle Ψ in the interval 108−188° (the equilibrium value is Ψ = 149.1°), and relaxing all the other degrees of freedom. We observe that the energy required by this deformation is relatively low (see Figure 2), and that the corresponding relaxation in the Φ angle does not exceed 2°. As expected, deforming the C1−O*−C1′ bending angle requires a significantly larger energy, as we verified by decreasing this angle from the equilibrium value (115.5°) to 99.4°, and measuring an energy increase of 8.2 kcal/mol (also in this case, all the other degrees of freedom have been relaxed).

Crystal

To identify the effect of the crystal environment on the trehalose molecule, and, more importantly, to investigate its interaction with water, we perform the DFT−MD structural optimization for the monohydrate crystal structure. Both in the experimental structure and in the relaxed one, the two trehalose molecules (and the two water molecules) in the crystal unit cell adopt the same geometry, and differ for their orientation only. The average distance between the starting positions (taken from ref 10) and those relaxed under the DFT−MD procedure turns out to be 0.08 Å for non-hydrogen atoms, and 0.24 Å for hydrogens.

TABLE 3: Intermolecular Hydrogen Bonds in the α−β Monohydrate Trehalose Crystal[a]

atoms	O−H distance	H−O distance	O−H−O angle
(*) O2−H1−O3′	1.017	1.601	177
O3−H3−O6′	1.019	1.647	168
(*) O4−H4−O_h	0.999	1.821	156
O6−H6−O2′	1.004	1.781	159
O2′−H2′−O_w	1.013	1.680	179
O3′−H3′−O3	1.018	1.641	173
O4′−H4′−O4	1.001	1.720	150
O_w−H_w−O2	1.007	1.684	171
O_w−H_w−O5′	0.990	1.975	170

[a] Trehalose atom numbers are defined in Chart 1, while the water atoms are indicated by the w subscript. Each of the hydrogen bonds listed is represented twice in the unit cell, which contains two equivalent trehalose and water molecules. An asterisk identifies bonds joining the planar structures discussed in the text. Distances are in angstroms and angles in degrees.

As expected, the cohesion of the crystal is mainly due to the formation of several intermolecular hydrogen bonds (see Table 3), which involve every hydroxyl group in the system. First of all, as already visible in the experimental geometry, but more apparent after our structural refinement, each water molecule gives rise to a pair of hydrogen bonds linking the two hydroxyl groups residing on the C2 and C2′ carbon atoms in the same trehalose molecule. The geometry of these two bonds, in which water is the proton donor on one side, and the proton acceptor on the other, is very similar, with angles and distances (d(O−H) = 1.68 Å, 170° ≤ θ(O−H···O) ≤ 180°) suggesting that these bonds are strong and relatively undistorted. The resulting trehalose−water complex (see Chart 2) represents a building block for the crystal significantly more symmetric than the isolated trehalose molecule.

The hydrogen atom of water not involved in the hydrogen bond described above gives rise to a slightly more distorted bond with the O5′ oxygen on a different trehalose molecule. Most of the remaining intermolecular hydrogen bonds join each trehalose molecule with its replicas in the adjacent crystal unit cells, thus giving origin to a nearly planar structure. The binding among the planes is provided by the few bonds identified by an asterisk in Table 3.

CHART 2: Structure of the Trehalose−Water Complex in the α−β Monohydrate Crystal

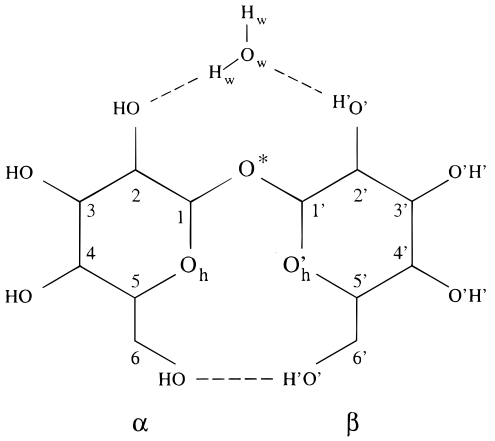

As a result of the formation of all these intermolecular hydrogen bonds, most of the hydroxyl groups adopt a different orientation with respect to the molecular geometry. Besides this obvious effect, the geometry changes induced by the crystal are rather small: as can be verified in Table 1, even bending and torsional angles do not change significantly in going from the molecule to the crystal. The most apparent effect is the decrease of the C1−O_h and C5−O_h bond asymmetry, which in the molecule was attributed to the anomeric effect. Interestingly, the C1′−O_h′ and C5′−O_h′ asymmetry is much less affected, despite the fact that the O_h′ oxygen is the acceptor for an intermolecular hydrogen bond, while O_h is not. Also noteworthy is the fact that the intramolecular hydrogen bond discussed above appears to be better defined in the crystal than in the isolated molecule, apparently because of different relaxations of the trehalose carbon backbone inside and outside the crystal.

Similarly to what we find for the structure, the most apparent difference between the vibrational spectra on the crystal and of the molecules concerns the modes localized on the OH groups. The OH stretching of water gives rise to two isolated peaks at 3141 cm^{-1} (the OH with the strongest H bond) and 3397 cm^{-1} (the OH with the weakest H bond). The pure OH stretching of trehalose gives rise to a band extending from 3155 to 3257 cm^{-1}, i.e., at lower frequency (again because of the formation of hydrogen bonds) and broader than in the gas-phase molecule. The CH stretching modes give rise to a band extending from 2860 to 3045 cm^{-1}, which, at variance from what we find in the molecular case, is contaminated by some OH stretching character. At 1630 cm^{-1} the isolated peak of the H−O−H bending of water appears. Below this frequency, the differences between the vibrational frequencies of the crystal and of the molecule are quantitatively small, and difficult to identify. Once again, the most apparent effect is an increase of the energy for the OH rotations around the minimum of the torsional potential, due to the formation of the intermolecular hydrogen bonds.

No experimental vibrational spectrum is available for either the gas-phase molecule or the monohydrate crystal. However, experimental information is available for the anhydrous α−α trehalose crystal and the dihydrate form[13] and for water solutions at various concentrations.[14] The computational results are consistent with the experimental data, although the differences in the systems considered by the experiments and by the computations prevent a very precise comparison.[15] In particular, the frequencies and the assignment reported in ref 13 for trehalose crystals are compatible with our results: all the frequencies computed in our study are well within the frequency intervals covered by the broad peaks displayed by the experimental spectra, and well-defined features (such as the highest frequency band, or the bands attributed to the CH bending) appear at nearly the same frequency in the computation and in the experiment, and therefore, they can be identified with confidence. The major difference between the experimental and the computational pictures is that the low-frequency modes ($\omega \leq 700$ cm^{-1}) provided by the DFT scheme are not so well defined and so localized to be associated with groups of two to three atoms, as done in the discussion of the experimental data reported in ref 13. Instead, as mentioned above, the character of each mode is progressively less well defined with decreasing energy of the mode.

For what concerns the water−trehalose liquid solutions, investigated by inelastic light scattering in ref 14, the computation for the monohydrate crystal suggests that both the top and the bottom of the OH stretching band are due to water, explaining the relative insensitivity of the width of this band to the trehalose concentration. Moreover, the band at 2800−3050 cm^{-1} observed experimentally in the water−trehalose solutions, but not in pure water, has to be attributed to CH stretching modes, in agreement with the results of our computation. Finally, the spectral feature at 1650 cm^{-1} is attributed to the bending of water, both by the experimental and by the computational analyses. A more detailed comparison requires DFT computations for systems with variable water−trehalose concentrations, which we plan to carry out in the future.

The frequencies and eigenvectors for the vibrational modes of the gas-phase trehalose molecule and of the monohydrate crystal are available from the authors.

Molecular Mechanics Models of Trehalose

Classical interatomic potentials represent the most practical models to study the thermal and dynamical properties of large assemblies of molecules, and therefore, they provide the most suitable tool to investigate the biological activity of trehalose at the atomistic level. Carbohydrates, and simple sugars in particular, are routinely modeled by the standard classical interatomic potentials for organic molecules, exemplified by the CHARMM and Amber recipes.[16] More specific force fields for carbohydrates have been obtained by tuning these basic models on specific properties of these molecules. To test their accuracy and reliability, we compared our DFT results to the predictions of one representative example of these models,[17] already used extensively in molecular dynamics simulations of trehalose solutions.[18] The geometry optimization and the harmonic frequency determination for the model potential have been carried out by the "Orac" program documented in ref 19.

First of all, we compared the results for the gas-phase molecule.[21] The results for the relaxed structure provided by the potential are in good agreement with the DFT data: the average difference between the results provided by the classical potential and by the DFT computation is 0.015 Å for the interatomic distances listed in Table 1, and 1.5° for the bending angles; torsional angles differ somewhat more, with the largest deviation (15°) measured for the Ψ torsional angle. Differences are also apparent in the orientation of the OH groups, resulting in a poor description of the intramolecular hydrogen bond O6′−H6′−O6 discussed above.

The structural analysis carried out for the gas-phase molecule has been repeated for the monohydrate crystal, giving very similar results: the major source of discrepancy between the molecular mechanics model and the DFT results (or the experimental structure) is the mediocre description of intra- and

inter-molecular hydrogen bonds. In particular, the O−H−O angles predicted by the molecular mechanics models can differ by more than 10° from their DFT counterpart. On the other hand, the molecular mechanics model predicts lattice constants and angles for the ground-state crystal unit cell to within 1% of the experimental values.

The comparison of harmonic vibrational frequencies and eigenvectors is less satisfactory than the comparison of ground-state structures, both for the isolated molecule and for the crystal. The model overestimates the frequency and underestimates the width of the high-frequency "bands" made by the OH stretching and bendings involving at least one hydrogen. Moreover, the characteristic features associated with the intramolecular hydrogen bond (the downward shift of the OH stretching mode, and the increase of the OH rotational energy) are absent, or not quantitatively reproduced. Also the energy ordering of the other modes with a clearly recognizable character is not well reproduced.

It is relatively easy to improve significantly the agreement of the model potential and DFT vibrational spectra by decreasing the force constants entering the definition of the molecular mechanics model. This improvement can be achieved without losing the good agreement in the ground-state structure, which is determined mainly by the equilibrium values of bond distances and angles.

Unfortunately, it is difficult to compare quantitatively, and possibly improve, the low-frequency modes, because it is difficult to identify them unambiguously in the broad band covering the 0−700 cm^{-1} range. The parameters providing a good fit for the medium- to high-frequency vibrational modes are available from the authors.

Discussion

Density functional computations with a recent and reliable approximation for the exchange and correlation have been performed for the gas-phase and monohydrate crystal of $\alpha-\beta$ trehalose. The structure has been fully optimized by the Car−Parrinello molecular dynamics, and the results are in good agreement with the experimental data. In addition, the computation provides a detailed picture for the vibrational properties, which can be used to interpret the available experimental data for trehalose crystals and solutions.

More importantly, the DFT data, reliable and internally consistent, can be used to test and refine classical interatomic potentials, which, at present, provide the most effective tool to investigate the transport, dynamical properties, and thermodynamics features of the water−trehalose system. A preliminary survey shows that existing models successfully reproduce the trehalose molecular structure, but their description of the intermolecular interactions (determined mainly by the geometry and strength of the hydrogen bonds) and of the harmonic dynamics is only moderately accurate. Simple adjustments in the potential parameters remove the most apparent discrepancies between the molecular mechanics models and the DFT computation. However, further DFT computations and systematic molecular dynamics simulations are required to verify the extent to which the improved models can reproduce quantitatively the structure of the hydrogen bond network in trehalose−water solutions.

Our study does not provide any direct insight into the atomistic basis for the biological role of trehalose. Additional studies, including the investigation of the interaction of trehalose with proteins and biological membranes, are required to clarify this problem. Nevertheless, the trehalose−water system has been extensively characterized by a variety of experimental techniques, and provides an additional important benchmark for the modelization of water−carbohydrate systems.

Acknowledgment. The DF calculations were performed on the Cray T3E computers in the Forschungszentrum Jülich, with generous grants of CPU time from the Forschungszentrum and the John von Neumann Institute for Computing (NIC).

References and Notes

(1) Stryer, L. *Biochemistry*, 4th ed.; Freeman: New York, 1995.

(2) Green, J. L.; Angell, C. A. *J. Phys. Chem.* **1989**, *93*, 2880. Magazú, S.; Maisano, G.; Migliardo, P.; Tettamanti, E.; Villari, V. *Mol. Phys.* **1999**, *96*, 381 and references therein.

(3) Waschipky, R.; Librizzi, F.; Nienhaus, K.; Cordone, L.; Nienhaus, G. U. *Biophys. J.* **1998**, *74*, A83. Cordone, L.; *et al. Biophys. J.* **1999**, *76*, 1043.

(4) For a review see: Jones, R. O.; Gunnarsson, O. *Rev. Mod. Phys.* **1989**, *61*, 689.

(5) Perdew, J. P.; Burke, K.; Ernzerhof, M. *Phys. Rev. Lett.* **1996**, *77*, 3865.

(6) Hamann, D. R. *Phys. Rev. B* **1997**, *55*, 10157. We are aware that, at present, the best description of hydrogen bonds is provided by an exchange-correlation functional belonging to the B3LYP family (Becke, A. *J. Chem. Phys.* **1993**, *98*, 5648. Lee, C.; Yang, W.; Parr, R. G. *Phys. Rev. B* **1988**, *37*, 785), mixing gradient-corrected approximations with exact exchange. These mixed schemes, however, are computationally much heavier than the approximation used in the present study.

(7) Troullier, N.; and Martins, J. L. *Phys. Rev. B* **1991**, *43*, 1998.

(8) Computations have been performed with the CPMD program version 3.0, Hutter, J.; *et al.*, Max-Planck-Institut für Festkörperforschung and IBM Research, 1990−1999.

(9) Car, R.; Parrinello, M. *Phys. Rev. Lett.* **1985**, *55*, 2471.

(10) Taga, T.; Miwa, Y.; Min, Z. *Acta Crystallogr.* **1997**, *C53*, 234.

(11) See, for instance, Singh, U. C.; Kollman, P. A. *J. Comput. Chem.* **1984**, *5*, 129.

(12) Montanari, B.; Ballone, P.; Jones, R. O. *Macromolecules* **1999** *32*, 3396.

(13) Gil, A. M.; Belton, P. S.; Felix, V. *Spectrochim. Acta, Part A* **1996**, *52*, 1649.

(14) Branca, C.; Magazu′, S.; Maisano, G.; Migliardo, P. *J. Phys. Chem. B* **1999**, *103*, 1347.

(15) We point out that the accuracy of the experimental data is far better than the one offered by DFT computations. However, trends and vibrational frequency differences among different forms of the same molecule are reliably predicted by these computations.

(16) See, for instance, Brooks, B.; *et al. J. Comput. Chem.* **1983**, *4*, 187. Cornell, W. D.; *et al. J. Am. Chem. Soc.* **1995**, *117*, 5179.

(17) Ha, S. N.; Giammona, A.; Field, M.; Brady, J. W. *Carbohydr. Res.* **1988**, *180*, 207.

(18) Liu, Q.; Schmidt, R. K.; Teo, B.; Karplus, P. A.; Brady, J. W. *J. Am. Chem. Soc.* **1997**, *119*, 7851.

(19) Procacci, P.; Darden, T. A.; Paci, E.; Marchi M. *J. Comput. Chem.* **1997**, *18*, 1848.

(20) A rotation of 180°, which could be considered a better choice, brings two hydrogens at short separation, thus giving a distorted estimate of the hydrogen bond energy.

(21) The atomic charges assumed by the model are fairly close to those computed by our DFT scheme.